Small Scintillating Cells as the Active Elements in a Digital Hadron Calorimeter for the e+e- Linear Collider Detector

A. Dyshkant[a]*, D. Beznosko[a], G. Blazey[a], D. Chakraborty[a], K. Frances[a], D. Kubik[a],
M. I. Martin[a], J. McCormick[a], A. Pla-Dalmau[b], V. Rykalin[a], V. Zutshi[a]

[a]Physics Department, Northern Illinois University, DeKalb, IL 60115

[b]Fermi National Accelerator Laboratory, Batavia, IL 60510

Abstract—**The ability to distinguish between hadronic W and Z decays is one of the most challenging requirements for the future Linear Collider Detector. Such sensitivity requires unprecedented jet energy precision, which may be possible with energy-flow algorithms. In energy-flow algorithms, energy clusters deposited by charged particles in a jet are identified by their energy distribution, and their energy is determined with a precise magnetized central tracker. The remaining jet energy from neutral particles can then be determined in the usual way with the hadronic calorimeter.   To distinguish energy clusters from individual particles, a calorimeter optimized for energy-flow must have fine lateral and longitudinal segmentation. Small scintillating cells with WLS fiber represent an attractive basis for a hadron calorimeter optimized for energy-flow. We present the expected jet resolution for such a device, based on Monte Carlo simulations. We then describe initial prototype studies.   In particular, systematic studies of cell performance under different combinations of manufacture and assembly, wavelength-shifting fiber types, reflective coating agents, splicing techniques, and photo-detectors are presented and discussed in detail.**

I. INTRODUCTION

THE current Tevatron run at Fermi National Accelerator Laboratory and the operation of the Large Hadron Collider (LHC) at CERN are clear priorities for the present and immediate future of the high-energy physics frontier. Simultaneously, preparation for the next step, a linear electron-positron collider (LC), has begun. A comprehensive feasibility study of a sampling hadron calorimeter with small scintillating cells has been undertaken at the Northern Illinois Center for Accelerator and Detector Development (NICADD). In this paper we report on preliminary prototypes of a digital hadron calorimeter (DHC) constructed from scintillating tiles with optical readout. The DHC would be a main component of the "small detector" for the proposed LC. After a short description of the envisioned detector system, we present results from a study of small scintillating cells with optical readout as the primary active element in a DHC. Section II describes the linear collider detector. Section III compares the simulated energy measurements for each cell (analog) with only the hit information (digital) of a scintillating hadron calorimeter. The main results regarding the tests of cell composition, shape and construction are presented in section IV. Conclusions are given in section V.

II. LINEAR COLLIDER DETECTOR

In the proposed Small Detector [1] (Fig. 1), active layers of the sampling hadron calorimeter are cylindrical, with radii from 1.44m to 2.46m and length of 5.72m. The entire device is immersed in a 5T magnetic field. Small cells (4-10cm^2) are primary elements of the active medium.

In this configuration, one square meter of active layer would consist of approximately one thousand identical cells. The cells are connected to photo-detectors via wavelength shifting (WLS) fiber either inside the strong magnetic field or outside with additional clear fiber. This type of calorimeter will have millions of independent channels with fast readout and good time resolution to avoid event pile-up. Because the average occupation per cell will be much less than one, the readout can be reduced to a single threshold (or bit) that detects the passage of a minimum ionizing particle (MIP). Single threshold detection simplifies the electronics and presumably reduces the overall detector cost. In addition, if light yield per MIP is

adequate, extruded rather than expensive cast scintillator can be used to reduce project costs.
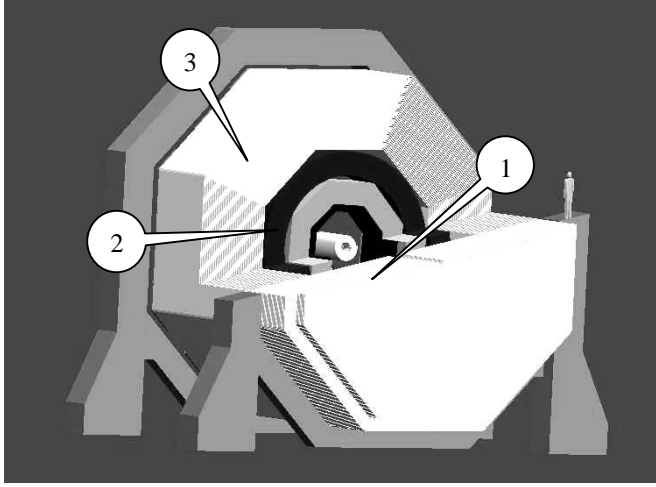

Fig. 1. Schematic view of the proposed Small Detector: 1 - Hadronic Calorimeter, 2 – Magnetic Coil, 3 – Muon System.

III. SIMULATIONS

In order to realize the full potential of a future linear electron positron collider [1], a detector must have jet energy resolution of $\sigma(E)/E = 30\%/\sqrt{E}$, where E is in GeV, or better [2] [3]. Most modern sampling hadron calorimeters have jet energy resolution on the order $\sim 90\%/\sqrt{E}$, which can be improved up to $\sim 50\%/\sqrt{E}$ using energy-flow algorithms (EFA) [2]. EFA resolution is further improved with a highly segmented hadron calorimeter.

The hits from charged particles can be separated from neutrals in a strong magnetic field by association with corresponding tracks in the inner volume. Subsequently, the tracker can be used to measure the charged components; an electromagnetic calorimeter measures the photons or electromagnetic energy; and the hadron calorimeter measures the remaining energy, primarily from neutral hadrons. Each device provides high-precision energy measurements. A hadron calorimeter with traditional resolution measures the energy of neutral hadrons only, which, on average, deposit approximately 11% of a jet's total energy. As the LC detector itself is optimized for EFAs, a net jet energy resolution of $30\%/\sqrt{E}$ should be achievable.

Figs. 2 and 3 show hit counts and energy resolution versus the energy of an incident charged pion for the simulated SD digital hadron calorimeter instrumented with square cells of area 2, 4, 6, 9, 12, and 16cm^2. In each run, all cells of the calorimeter had the same area. A cell is "hit" by a particle if the energy exceeds 0.25 MIP.

To evaluate jet energy resolution in an algorithm-independent fashion, stable, generated MC particles were clustered into 0.7 simple cone jets. Constituent energies were smeared using the following prescription:
a. Charged particles were not smeared at all.
b. Photons were smeared with a $17\%/\sqrt{E}$ sampling term.
c. Neutral hadrons were smeared using the fractional resolution shown in Fig. 3 for the 3x3cm^2 cells.

The energy of jets with and without smearing is compared to obtain the parameterized jet energy resolution, as it is shown in Fig. 4.

Strong correlation between the number of hits and incident energy is required for a single threshold or single bit DHC to measure energy. The resolution curve indicates that digital and traditional analog calorimeters have comparable performance. In fact, the results show the DHC to be superior below 10 GeV. In any event, the comparable analog resolution, coupled with the superior segmentation, is necessary for the success of a DHC.
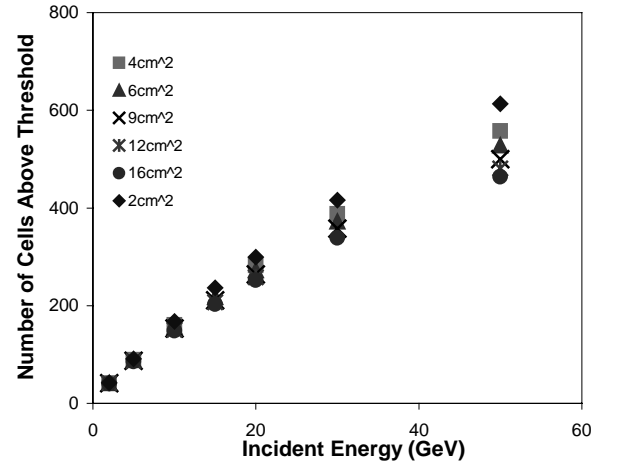

Fig. 2. Number of hits above threshold (0.25 MIP) versus charged pion incident energy for various DHC cell sizes.
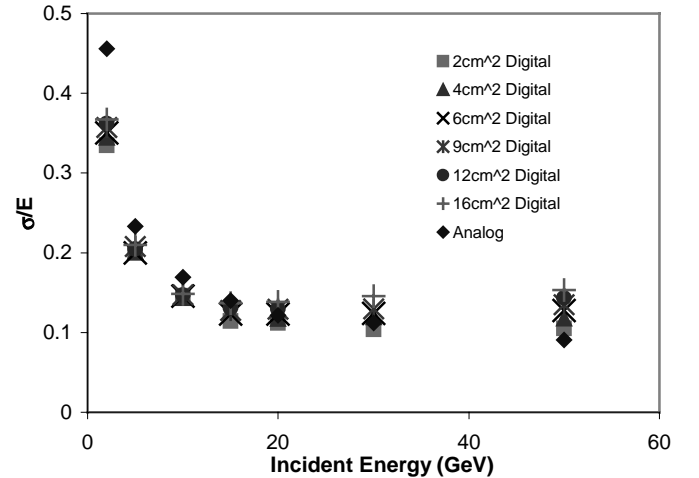

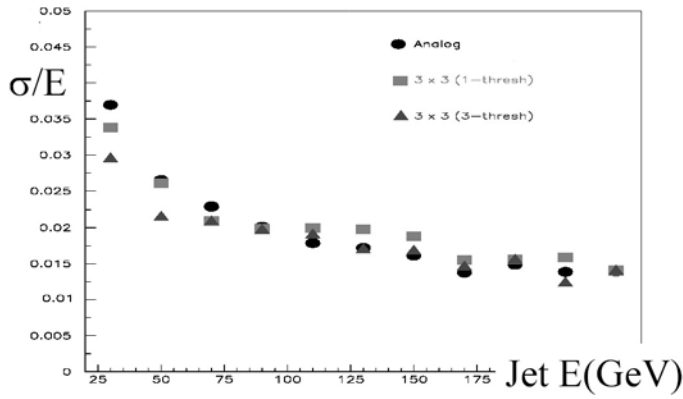Fig. 3. Energy resolution versus the incident energy of single charged pions.

Fig. 4. Energy resolution for jets

IV. PROTOTYPING THE SCINTILLATING CALORIMETER

The Scintillating Digital Hadron Calorimeter (SDHC) prototype shown in Fig. 5 consists of the following major components: scintillating cells, optical fibers, photo detectors, and passive material. The prototype tower is a stack of twelve active layers. Each active layer, shown in the left top corner of Fig . 5, is an array of seven identical hexagonal cells. Each cell has dimensions [4] close to the Moliere radius of brass, which is ~17mm. The arrays are read out with six Hamamatsu H8711 assemblies [5] (multi-anode photomultiplier tube (MPMT) that has 16 channels) via 1m long WLS fibers connected to clear fibers with optical connectors. Each passive layer is a 125x125x25mm brass plate. The prototype was tested with cosmic rays. Before discussing results, the unit cells will be described in detail.
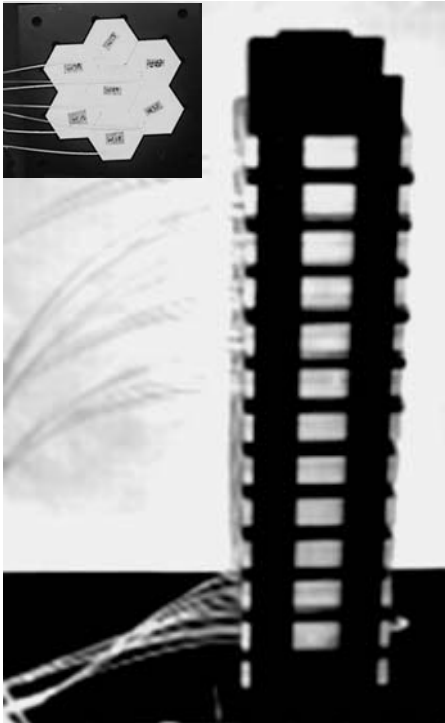

Fig. 5. NICADD prototype scintillating digital hadron calorimeter tower. In the top left corner a photograph of cell array is shown.

A. OPTICAL FIBERS

The following optical fibers were tested for the readout:
- Saint-Gobain [6] BCF-92, square, 0.9mm;
- Saint-Gobain BCF-92, round, 0.9mm OD;
- Saint-Gobain BCF-92, round, 1.0mm OD;
- KURARAY [7], Y-11, S type, round, 0.94mm OD, multiclad;
- KURARAY, clear, S type, round, 0.94mm OD, multiclad;
- KURARAY, Y-11, S type, round, 1.00mm OD, multiclad.

All fiber ends were polished using the fly diamond cutting technique, and one end of each WLS fiber was aluminum-mirrored. All fibers were 1m long. At least one hundred of each type was tested.
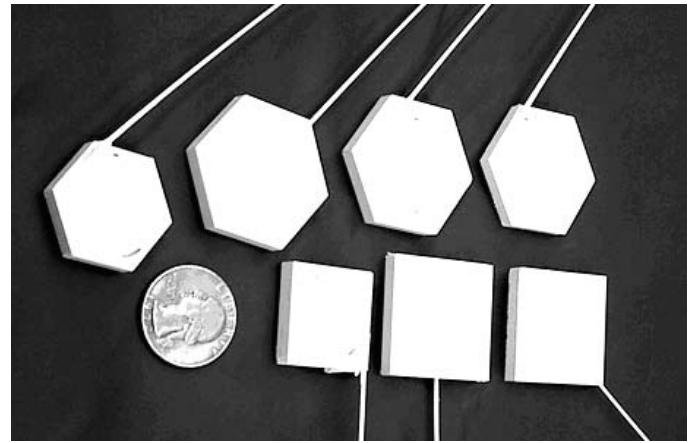

Fig. 6. The different species of cells were thoroughly investigated along two perpendicular directions, as shown in schematics for each cell geometry below.

Since the WLS fiber must be inserted in a scintillator cell (Fig. 6), the response as a function of bending radii is a critical parameter. The light loss from bending for BCF-92 round, 0.9mm diameter fiber was measured using the light created in a scintillating cell with a ^{90}Sr radioactive source (Fig. 7).
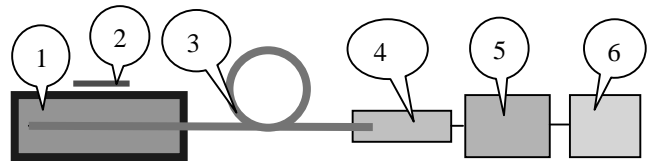

Fig. 7. Schematic of apparatus to measure WLS response as a function of curvature: 1 is a scintillating cell; 2 is a radioactive source ^{90}Sr; 3 is a circular fiber loop; 4 is a photomultiplier tube R-580 [5]; 5 is a pico-ammeter [8]; and 6 is a PC based data acquisition system.

The end of the fiber not embedded in the cell was manipulated into circular loops of varying radii. All parts of the fiber outside of the loop were straight and fixed to the bench. The response was measured for different loop inner

diameters. Straight fiber response was considered as zero bending loss. Fig. 8 shows the light loss for different loop diameters. For loop diameters less than 25mm, the light losses due to bending increased exponentially.
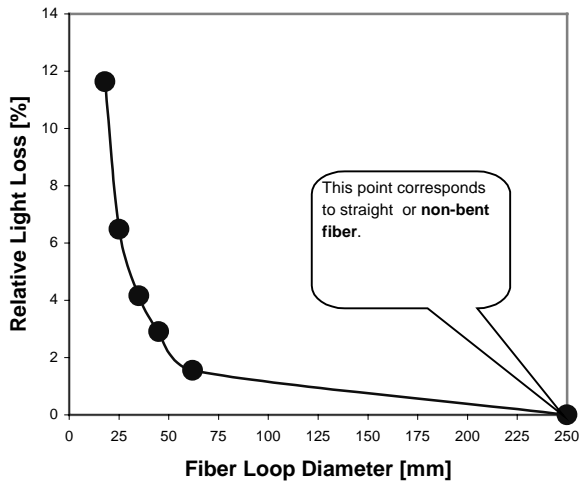

Fig. 8. Bending light loss for round 0.9mm diameter BCF-92 fiber

If the photo detectors are not placed inside the calorimeter, WLS fibers must be connected to clear fibers via optical connectors or splicing. Thermal splicing of WLS fiber with clear fiber was successfully performed for KURARAY round 0.94mm fibers, following procedures established by thecmS collaboration [9]. Round, 1mm diameter, KURARAY, Y-11, WLS fibers with multi-cladding provided a response which was 3.14 times larger than the output from 0.9mm BCF-92.

B. SCINTILLATING CELL THICKNESS

The following materials were used to fabricate scintillating cells:
- Saint-Gobain [5] BC-408; 5, 10, and 20mm thickness;
- Eljen Technologies [10] EJ-200; 3, 4, and 5mm thickness;
- NICADD-Fermilab extruded [11] 5mm thickness.

Cell response versus thickness was studied for cells of 3 to 5mm thickness. The cell area was 9.4cm² and cell itself is of regular hexagonal shape. Each cell had a WLS fiber inserted into a sigma shaped groove. (Hexagonal ones are preferred due to a more uniform response and less edge effect compared to cells with other shapes, such as a square.) Because the thickness range was small, all cells were made from the same strip of cast scintillator, with an initial thickness of 5.5mm.

The response as a function of thickness is shown in Fig. 9, where each point represents the average response of eight cells. Units for response were normalized to 3mm thick cells, in order to simplify analysis. A ^{137}Cs radioactive source was used.

The response is a linear function of cell thickness up to 5mm. The accuracy of measurement at each point was ±2%.

To quantify the effect of cell surface machining on response, three sets of similar cells with polished or machined top or bottom surfaces were tested. The results are summarized in Table I. The accuracy of measurement at each point was ±2%. The average responses were virtually identical, so surface treatment has no significant affect on cell response.
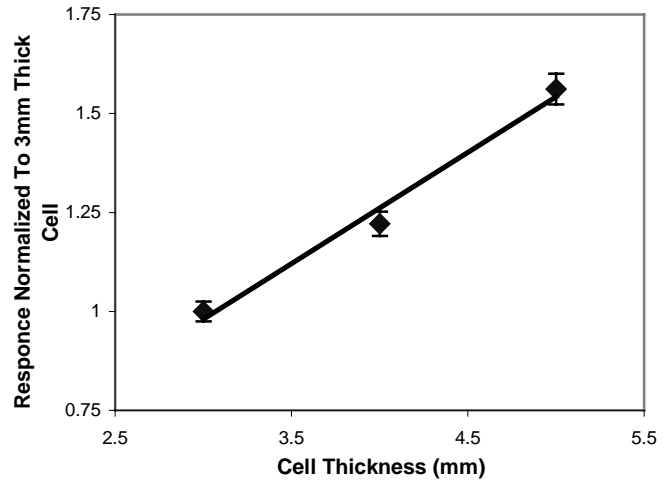

Fig. 9. Response of cells with thicknesses of 3, 4, and 5mm.

TABLE I
NORMALIZED RESPONSE OF CELLS FOR DIFFERENT KINDS OF SURFACE TREATMENTS

Surface treatment	Unpolished top and polished bottom	Polished top and polished bottom	Unpolished top and unpolished bottom
Response	0.98	1.00	1.02

C. WRAPPING AND COATING

Cell response as a function of surface treatment, such as coating or wrapping was tested. Tyvek has been traditionally used to cover scintillating tiles. For millions of small cells painting is an attractive alternative. It is less labor intensive than manually wrapping each cell in Tyvek. Also, the same reflective properties that capture the light inside the cell, reduce optical crosstalk between the cells, and provide a reflective outer surface that can serve as a target for metrology.

The following geometry, materials, and tools were used to test surface treatments:
1. Cells were made out of 5mm thick BC-408 scintillator, with hexagonal shape and area of 9.4cm²; five out of 11 had polished edges.
2. The cell groove was sigma-shaped with a rectangular cross-section, 12mm radius, 1mm width, 4.5mm depth,

and a angled exit. A 25° arc of the circle that corresponds to the position of the groove, is without a groove. The groove for the WLS fiber must be angled; otherwise, the cells cannot be connected to each other without additional gaps (dead zones) between sides.

3. The WLS fibers were square BCF-92 with 0.9mm sides, embedded and glued into the groove using BC600 optical glue.

4. Wrapping or coating materials were Tyvek, CM500, VM2002, and CM590 radiant light films from 3M [12], aluminized Mylar, titanium white acrylic paint from Liquitex [13], and aluminum foil. Artists' titanium dioxide white acrylic paint from Liquitex was used for the tests described below. (Saint-Gobain BC-620 reflective paint did not provide a firm surface.)

5. The photo multiplier tube was a HAMAMATSU [7] R580, with a high voltage of 1300V applied; dark current was less than 0.07nA, or less than 0.1%, for regular measurements with ^{90}Sr (2mCi). Current was measured with a Keithley pico-ammeter [8] interfaced to a PC via GPIB.

Normalized cell responses for different coatings or wrappings are summarized in Table II. All measurements were made with the same cells that were consecutively wrapped in each material and then finally painted in white acrylic. Super-reflective film provided the best response. Painted cells had a response of 10-15% less than Tyvek-covered cells.

Response comparisons between coated or wrapped cells with polished versus non-polished sides are shown in Table III. The accuracy of averages for these measurements was 3%. For common coating or wrapping materials, cells with non-polished sides provided 30% greater response than cells with polished sides. For higher response, the cell treatment choice for the sides was more important than for surfaces.

TABLE II
NORMALIZED CELLS RESPONSE FOR DIFFERENT COATING OR WRAPPING

Coating	Tyvek	Paint	VM2002	Mylar
Response	1.00	0.89	1.08	0.83
Coating	CM590	CM500	Alum. Foil	
Response	0.28	0.44	0.63	

TABLE III
RATIO OF RESPONSE FOR CELLS WITH UNPOLISHED SIDES TO THE RESPONSE OF CELLS WITH POLISHED SIDES

Coating	Tyvek	Paint	VM2002	Mylar	CM590	CM500
Ratio	1.27	1.30	1.28	1.30	1.14	1.19

We also measured the response of mirrored cells with the hope that such treatment could provide minimal dead zones and low optical cross talk between cells. The response was compared with cells wrapped in Tyvek, painted with BC-620, wrapped in glued mirrored tape, or painted in black ivory. The results are summarized in Table IV. The mirrored cells

provided, on average, four times less response than cells wrapped in Tyvek. The very low response of cells painted in black illustrates the importance of surface treatment.

TABLE IV
NORMALIZED CELL RESPONSE FOR DIFFERENT COATING MATERIALS

Type of coating/wrapping	Relative response
Tyvek	1.00
Glued Aluminized Mylar Tape	0.48
Aluminum Sputtering	0.24
Paint BC620	0.98
Paint White Acrylic	0.90
Paint Black Acrylic	0.06

Gaps between the cells edges significantly reduce the efficiency of particle registration. Therefore, the thickness of paint should be small. On the other hand, if the thickness of the paint is insufficient, the cell response will be reduced and optical crosstalk between cells will be high. Thus, the thickness of the paint must be optimized. If the white-acrylic paint thickness was more than 0.2mm, the optical crosstalk to adjacent neighbors was negligible.

D. OPTICAL CROSSTALK BETWEEN CELLS

Optical crosstalk or "light leaks" between cells penetrates from one cell to another through the sides. If the level of optical crosstalk is higher than the threshold, it will be detected as a particle. This kind of noise can hamper reconstruction of the events. The measurement described below shows crosstalk to be about 1%.

Optical crosstalk was measured with an array of seven cells. Six neighbors surrounded the central cell. A 5mCi ^{90}Sr radioactive source was used to generate light in the central cell. Tedlar film was used to wrap the central cell so that optical crosstalk from the central cell to the neighboring cells was impossible. These measurements were performed with a Hamamatsu PMT R-580 instrumented with an optical mixer. The WLS fibers were connected to the PMT via square plastic ferrules with 4.2mm sides. The mixer reduces the non-uniformity across the PMT photocathode to less than 0.1%. The current measurements were performed using a Keithlay picoammeter. The dark current was 0.4nA, or 0.02%. Table V shows the normalized responses. The accuracy of these measurements was 0.5%. The first row in the Table V shows that crosstalk must be less than 1.000 – 0.958 = 0.042 or 4.2%.

The second row in Table V shows that wrapping in black Tedlar reduced the brightness of the foreground from 0.985 to 0.960 or by 0.025 (2.5%). A correction is needed to the level of measured crosstalk, because the central cell brightness is not a constant value: 0.042 – 0.025 = 0.017. The level of response with Tedlar wrapping and a disconnected central cell (the third

row in the table) shows that the amount of light directly generated by radioactive source in all neighboring cells (radioactive background) is 0.006.

	Central cell wrapped in Tedlar (crosstalk impossible)	Central cell not wrapped in Tedlar (crosstalk possible)
All seven cells connected to PMT	0.958	1.000
Only central cell connected to PMT	0.960	0.985
Only neighbor cells connected to PMT. Central cell disconnected.	0.006	0.008

This background should be subtracted from the level of crosstalk: 0.017 – 0.006 = 0.011. These calculations show that the level of optical crosstalk is 1.1%.

E. CELL SHAPE, AREA, and GROOVE

Response as a function of shape and area was measured with hexagonal and square cells of 1.2mm width with angled sigma grooves for the WLS fibers and areas of 9.4, 6.0, and 4.0cm². The angled groove starts at a depth of 4.5mm and becomes progressively shallower to zero mm at the exit. Eight cells were used for each measurement. Measurement accuracy was better than ±2%. The results are given in Table VI. The comparison shows that cell responses are not sensitive to the cell's area or shape. No cracks in WLS fibers were detected, even in the smallest cells (6cm² area) with sigma groove.

Shape and area	Hexagon 9.4cm²	Square 9.4cm²	Hexagon 6.0cm²	Square 6.0cm²	Square 4.0cm²
Response	1.00	0.95	0.93	0.93	0.85

Response was also measured with hexagonal cells made from cast EJ-210 and extruded NICADD/FNAL scintillator with sigma grooves. The extruded scintillator had a response 60 ± 0.02 % that of cast scintillator [11], [14].

The effect of groove type was also tested for straight groove, nominal sigma shaped fiber groove, angled groove, and round, extruded holes with embedded and glued WLS fibers. The results for 9.4cm² cells are shown in Table VII. The data is normalized to the average response of a hexagonal cell with an angled sigma groove. These measurements used the NICADD-

FNAL extruded scintillator with 4.87mm thickness. A ^{90}Sr radioactive source was placed in the center of the cells.

Cell Shape	Hexagon	Hexagon	Square
Groove for WLS fiber	Sigma	From Corner to Corner Extruded Hole	From Side to Side Extruded Hole
Response	1.00 ± 0.02	0.89 ± 0.02	0.85 ± 0.03
Uniformity	Uniform	Non uniform	Non uniform
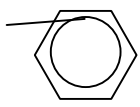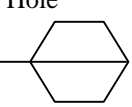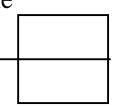
F. UNFORMITY

The uniformity of cell response with straight or sigma grooves was measured. The cell shape, together with the shape of the groove, defines the unique response to a charged particle. A mapping of cell response provides information for choosing the electronic threshold and comparing cell designs. The scanned cells had the same area (9.4cm²) and thickness. A ^{90}Sr radioactive source with a 2mm collimated slit was used for these measurements. The accuracy of the source positioning was 0.2mm. For uniformity measurements, the cell was flipped, leveled, and put on a soft surface to protect the WLS fiber. The collimated source was moved along the bottom surface of the cell. The tests are enumerated in Table VIII and detailed plots are presented in Appendix A.

Cell shape and WLS fiber groove type	Figure
Hexagonal with extruded hole	A1
Square with extruded hole	A2
Square with angled sigma groove	A3
Hexagonal with angled sigma groove	A4
Square with straight angled groove	A5
Two hexagonal cells with sigma groove	A6

The cell response maps show that an electronic threshold of 0.25 MIP is sufficient. Dead zones and edges around a cell reduce response uniformity; however, these effects can be reduced with lower thresholds.

G. LIGHT LOSS IN THE CELL DUE TO AGING

To examine light yield as a function of time, the response measurement was repeated frequently for 4-6 months after

production.. The measurements were made with 30 hexagonally shaped cells with 9.4cm² area and Kuraray, 1mm diameter, Y-11, multiclad, S-type WLS fibers glued inside the angled sigma groove. Within errors, the response was stable over the entire period. The average response after 6 months was 0.993 ± 0.006 the response at the time of production.

H. PHOTO DETECTORS

The prototype stack shown in Fig. 5 was read out using a trigger to select particles with tracks perpendicular to the stack. The system used a V792N series QDC from CAEN [15] and a LabVIEW-based DAQ system. Fig. 10 shows the MPMT response for a MIP [16]. The peak between the pedestal and ~212 QDC counts is due to crosstalk from adjacent channels of the MPMT. Fig. 11 shows the response of the same MPTM channel, but for light-emitting-diode signals, which were significantly attenuated with gray optical filters in order to obtain a single electron spectrum. Analysis of these plots shows that the MPMT peak in Fig. 10 corresponds to ~10 photoelectrons per MIP per cell [17]. Clearly, a 0.25 MIP threshold is well within the capabilities of these scintillator cells.
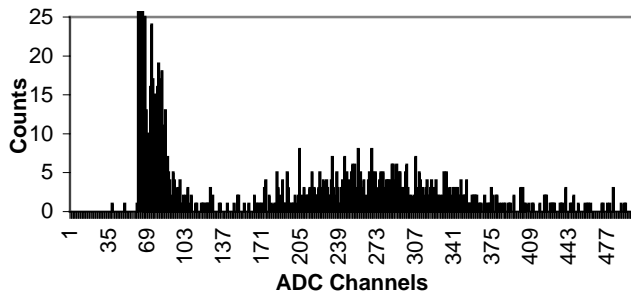
Fig. 10. Cell and MPMT H8711 response to a MIP.
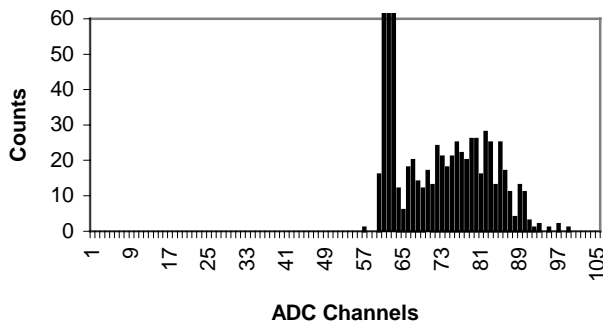
Fig. 11. Response of LED signals significantly attenuated with gray optical filters in order to obtain a single electron spectrum for H8711.

Operation of the SDHC within a strong magnetic field, essential for the EFAs, excludes the use of standard photomultiplier tubes. New photo detectors, such as the SiPM ("Pulsar" Enterprise [18], Russia) or the MRS ("CPTA" [19], Russia), offer very attractive possibilities – especially the

insertion of the photo-detectors onboard the scintillator due to their miniature sizes. For these sensors we performed preliminary comparative amplitude measurements of the output response with the same light flux at the input. The working points of both devices were chosen at the same noise count rate. Two distributions are shown in the Appendix B. Currently we are undertaking a detailed study of both promising candidates.

V. CONCLUSIONS AND OUTLOOK

Simulations show that a scintillator based digital hadron calorimeter can provide performance comparable to a fully analog calorimeter. Small scintillating cells with optical readout, needed for an HCAL, were studied with radioactive sources and cosmic rays. Based on our studies a nominal cell element with 9.4cm² area, hexagonal shape angled sigma groove, and KURARAY, Y-11, multiclad, S-type, 1mm diameter WLS fiber readout would meet the requirements of a DHC. Using PMTs or SiPM, these cells provide ~10 photoelectrons per MIP (measured with cosmic rays). Further R&D will be needed in the following areas: production, assembly, choice of photo detector and electronics, and optimization of cell area. We plan to construct a test beam prototype and continue studies of the energy flow algorithms.

VI. APPENDICES

A.

Figs. A1 present the normalized uniformity response for a hexagonal cell. The cell with 38mm length and 32mm width was made from an extruded scintillating strip [11] with an inside oval hole (2.1-2.8mm diameter) for the WLS fiber readout. Scans were performed along and across the WLS fiber embedded into the cell as shown by the dashed lines in Fig. A1a.
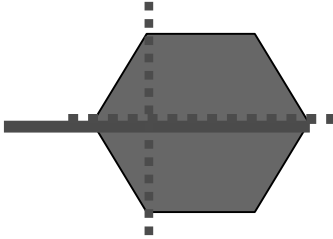

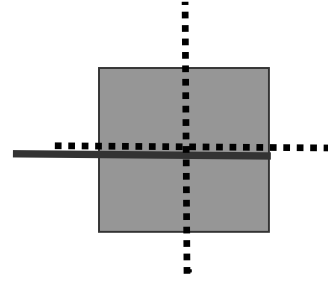Fig. A1a. A schematic of the hexagonal cell with WLS fiber (the green line) embedded and glued inside an extruded hole. Dashed lines represent the scan directions.
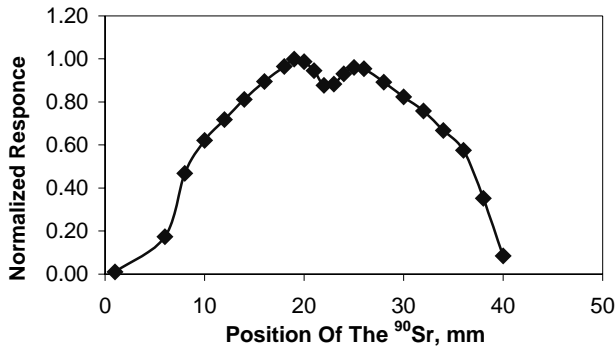
Fig. A1b. Normalized response for a scan performed across the fiber of a hexagonally shaped cell. The response was symmetric and up to 40% non-uniform near the edges.
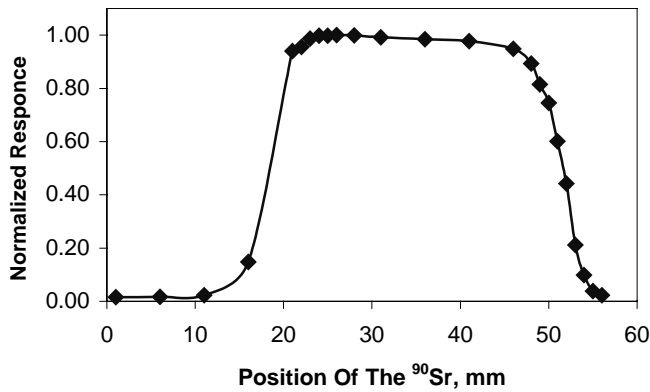
Fig. A1c. Normalized response for a scan made along the fiber of a hexagonally shaped cell. The response was uniform with a small decrease at the mirrored fiber end.

Figs. A2 present the normalized uniformity response for a square cell. The cell was made from extruded scintillating strip [11] with an inside oval hole (2.1-2.8mm diameter) for the WLS fiber.

Fig. A2a. A schematic of the square cell with WLS fiber (the black line) embedded and glued inside the extruded hole. The dashed lines represent scanning paths.
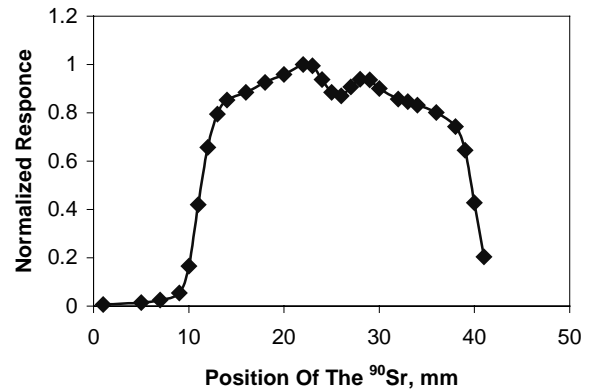

Fig. A2b. Normalized response for a scan performed across the fiber of square shaped cell. The response is up to 20% non-uniform at the edges.
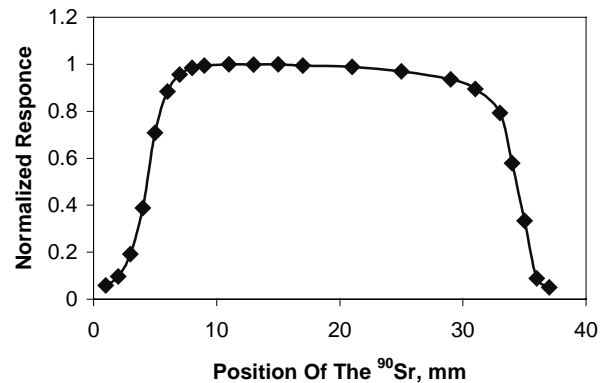

Fig. A2c. Normalized response for the scan made along the fiber of the square shaped cell. The response is uniform with small slope near the mirrored end of the fiber.

Figs. A3 present the normalized uniformity response for a square cell. The cell was made from cast scintillator [8] with a 1.2mm wide, angled sigma groove for the WLS fiber.
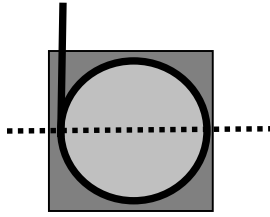

Fig. A3a: A schematic of the square cell with WLS fiber (the black line) embedded and glued inside the angled sigma groove (the black line). The minimum distance between the edge of cell and the sigma groove is 1mm. 30% of the cell area (darker in the picture) is out of the sigma groove.
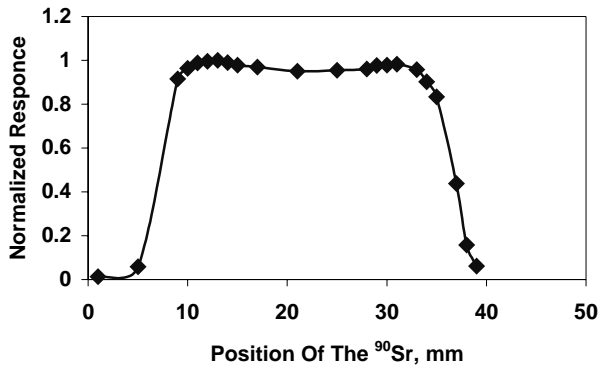

Fig. A3b. Normalized response for the scan performed across a square shaped cell with the angled sigma groove for WLS fiber. The response is uniform with a 5% deviation at the center.

Fig. A4 presents the normalized uniformity response for the hexagonally shaped cell shown in Fig. A4a. The cell was made from cast scintillator [11] with a 1.2mm wide angled sigma groove for the WLS fiber.
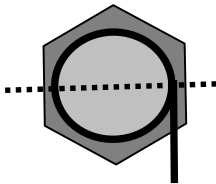

Fig. A4a. A schematic of the hexagonally shaped cell with WLS fiber embedded and glued inside the angled sigma groove (the black line). The minimum distance between the edge of cell and the sigma groove is 1mm. 20% of the cell area is outside sigma groove (darker area in the picture).
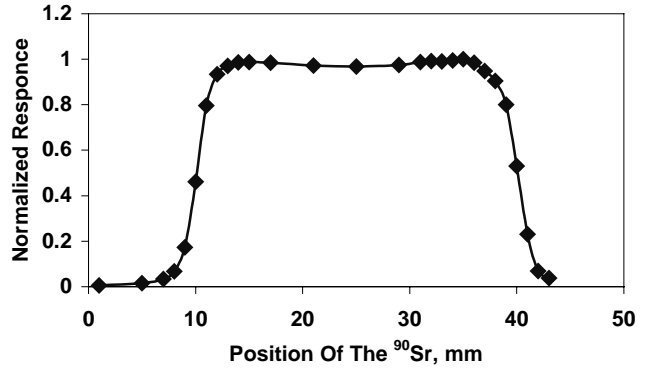

Fig. A4b. Normalized response for the scan performed across the hexagonally shaped cell with a angled sigma groove for WLS fiber. The response inside the groove circle is highly uniform with a 3% deviation in the center.

Figs. A5 present the normalized uniformity response for a square cell. The cell was made from cast scintillator [8] with 1.2mm wide angled straight groove for the WLS fiber.
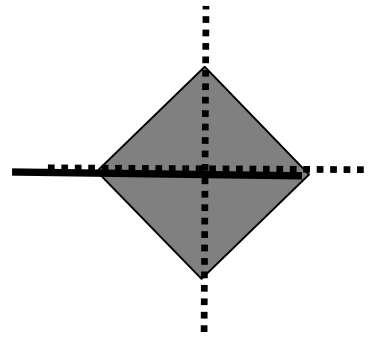

Fig. A5a. A schematic of the square cell with WLS fiber (the black line) embedded and glued inside the angled straight groove. Dashed lines represent scan directions.
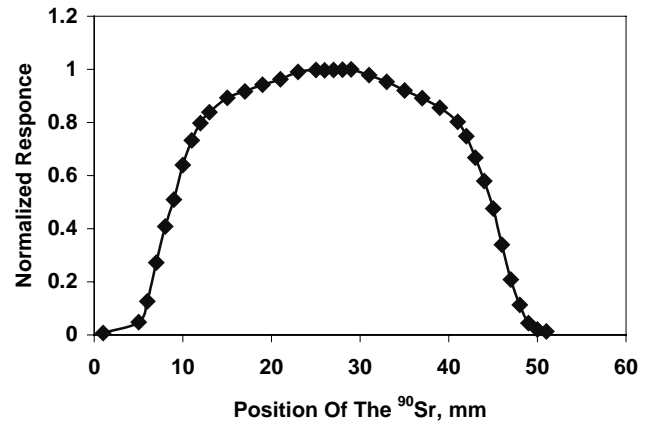

Fig. A5b. A normalized response for the scan performed across the square shaped cell with an angled straight groove for the WLS fiber.
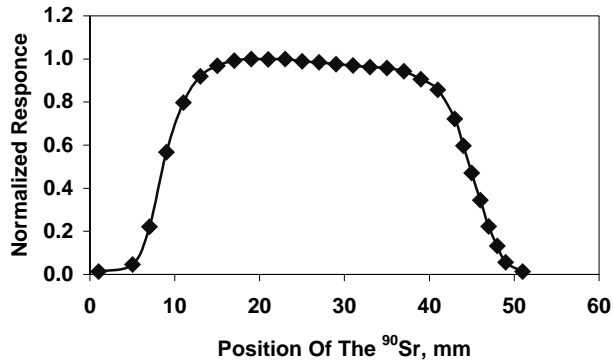
Fig. A5b. A normalized response for the square shaped cell with an angled straight groove for the scan performed along the WLS fiber.

Figs. A6 presents the normalized uniformity response for two hexagonally shaped cells with WLS fibers connected to the same photomultiplier tube.
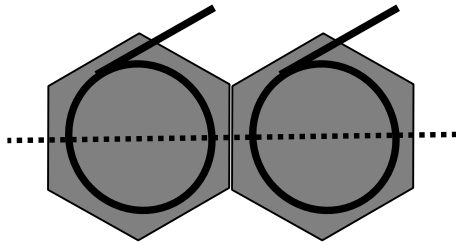

Fig. A6a. A schematic of the hexagonally shaped cells with WLS fiber (the black line) embedded and glued inside the sigma grooves. Dashed line represents the scan direction.
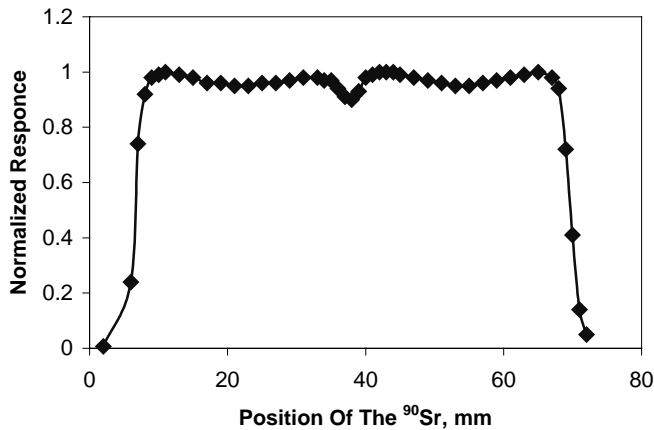

Fig. A6b. Normalized response for the scan performed across the hexagonally shaped cells with sigma grooves for the WLS fiber readout. The curve represents the summed response for the two cells

B.

The two graphs below present the response of a MRS and a SiPM to the same signal from a Light Emission Diode (LED). Both detectors are positioned at the same working point. The point for each detector was chosen based on noise studies – i.e. at corresponding bias voltages each device produced similar noise counting characteristics close to each other in frequency and in amplitude distribution.

Fig B1 shows the response of the MRS with an average of ~4.5 Photo Electrons (PE). Fig B2 presents the response of the SiPM to the same signal; it shows clear PE separation but only ~2.5PE which is less then the MRS responce. Precise PE count was obtained by statistical analysis of the plots but could also be counted.
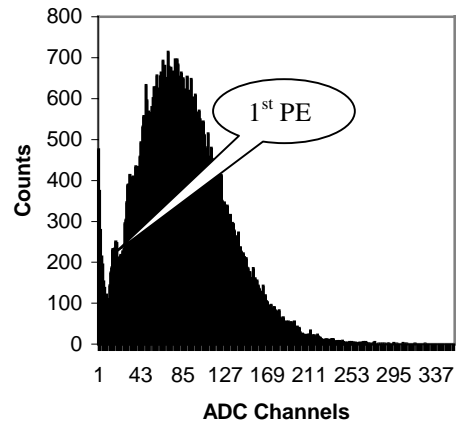

Fig. B1. MRS response at 51V bias voltage to LED signal. Pedestal is in 1st channel.
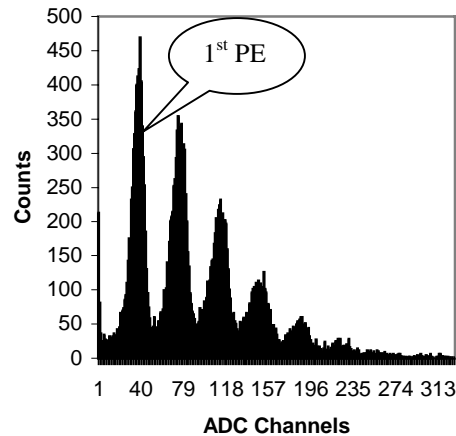

Fig. B2. SiPM response at 57V bias voltage to LED signal. Pedestal is in 1st channel.

VII. Acknowledgment

VIII. References

[1] C.Damerell et al., pg. 431, and J.Brau et al., pg. 437, Proc. Swnowmass 1996.
J. Jaros, Silicon Detector Tracking, ALCPG Workshop Cornell, July 15, 2003.

[2] O. Lobban et al., On the Energy Measurement of Hadron Jets, Proceedings of the Tenth International Conference on Calorimetry in Particle Physics, Pasadena, 2002. World Scientific, Singapore, 2002, p.814-833.

[3] TESLA Technical Design Report, DESY, March 2001.

[4] V. Morgunov, Calorimetry Design with Energy-Flow Concept (Imergin Detector for High Energy Physics), Proceedings of the Tenth International Conference on Calorimetry in Particle Physics, Pasadena, 2002. World Scientific, Singapore, 2002, p.70-84.

[5] HAMAMATSU CORPORATION, 360 Foothill Road, P.O.BOX 6910, Bridgewater, NJ 08807-0919, USA; 314-5, Shimokanzo, Toyooka-village, Iwata-gun, Shizuoka-ken, 438-0193 Jap1.

[6] SAINT-GOBAIN (Bicron), 12345 Kinsman Road, Newbury, OH 44065, USA.

[7] Kuraray America Inc., 200 Park Ave, NY 10166,USA; 3-1-6, NIHONBASHI, CHUO-KU, TOKYO 103-8254, JAPAN.

[8] Keithley Instruments, Inc., 28775 Aurora Road, Cleveland, OH 44139, USA.

[9] CMS. The Hadron Calorimeter Project Technical Design Report CERN/LHCC 97cmS TDR 2, 20 June 1997.

[10] ELJEN TECHNOLOGY, PO Box 870, 300 Crane Street, Sweetwater, Texas 79556, USA.

[11] Anna Pla-Dalmau, Alan D. Bross, Victor V. Rykalin, Extruding Plastic Scintillator at Fermilab, FERMILAB-Conf-03-318-E, October 2003.

[12] 3M Light Management Ventures, 3M Center, Building 0223-01-N-12, St. Paul, MN 55144-1000.

[13] 2000 Liquitex Artist Materials, P.O. Box 246, Piscataway, New Jersey, 08855 USA.

[14] The MINOS Detectors Technical Design Report. NuMI-L-603, March 1, 1999.

[15] CAEN, in USA – W-IE-NE-R Plein & Baus Corp., 300 East Auburn Ave., Springfield, OH 45505.

[16] K. Francis, Evaluating Small Scintillating Cells for Digital Hadron Calorimeter, Unpublished Master's Thesis, NIU, DeKalb, IL, October 2003.

[17] A. Bross et al., The Digital Hadron Calorimeter (DHC) Elements Test, FERMILAB-TN-733, April 2003.

[18] G. Bondarenko et al., Nucl. Instr. and Meth., A242 (2000) p.187

[19] V. Golovin et al., Limited Geiger-Mode Silicone Photodode With Very High Gain. Nucl.Phys.Proc.Suppl. 61B: 347-352, 1998.